Systematic DC/Small-Signal/Large-Signal Analysis of Heterojunction Bipolar Transistors Using a New Consistent Nonlinear Model

Rached Hajji, *Member, IEEE*, Ammar B. Kouki, *Member, IEEE*, Sayed El-Rabaie, *Member, IEEE*, and Fadhel M. Ghannouchi, *Senior Member, IEEE*

***Abstract*—In this paper, a new systematic approach to heterojunction bipolar transistors (HBT's) characterization and modeling is presented. The proposed approach is based on a new compact HBT nonlinear circuit model which accounts for both self-heating and the temperature dependence effects. The model's parameters are extracted from measured dc-IV characteristics and S-parameters. The power characteristics of the device are then predicted using the extracted model without any further optimizations. The same model is also used for intermodulation distortion analysis. The model has been implemented in a number of commercial nonlinear simulators and in an in-house computer code. Results are presented for two different size devices showing good agreement with measurements.**

NOMENCLATURE

I_b	Base-emitter current
V_{ce}	Collector-emitter voltage.
I_s	Base-emitter saturation current.
$\alpha = 1/(\eta V_t)$	Diode fitting parameter.
I_c	Collector current X_1 to X_{10}; collector current fitting parameters.
I_{bo}	Base reference current.
I_{bn}	Normalized base current.
T_o	Reference temperature.
T	Analysis temperature.
C_{be}	Intrinsic base-emitter capacitance.
C_{bc}	Intrinsic feedback base-collector capacitance.
a_1, a_2	Fitting parameters for the bias-dependent base-emitter capacitance, C_{be}.
b_1, b_2	Fitting parameters for the bias-dependent base-collector capacitance, C_{bc}.
C_{pbc}	Extrinsic base-collector capacitance.
R_b, R_c, R_e	Contact resistance for base, collector, and emitter.
L_b, L_c, L_e	Leading pads inductances for base, collector, and emitter.
C_{pb}, C_{pc}	Leading pads capacitances for base and collector.
L_{bo}, C_{bo}, L_{co}, C_{co}	Packaging parasitics.

Manuscript received November 28, 1994; revised November 12, 1995. This work was supported in part by the Natural Science and Engineering Research Council of Canada (NSERC).

R. Hajji. A. B. Kouki, and F. M. Ghannouchi are with the Electrical and Computer Engineering Department, École Polytechnique de Montréal, Succ. Centre-Ville, Montréal, Quebec, Canada, H3C 3A7.

S. El-Rabaie is with the Faculty of Engineering, 32952 Menouf, Egypt.

Publisher Item Identifier S 0018-9480(96)01434-2.

I. INTRODUCTION

THE HETEROJUNCTION bipolar transistor (HBT) devices are becoming increasingly more popular in microwave and millimeter-wave power applications. These devices are attractive for their power density capability, linearity, and high cut-off and oscillation frequencies, which have been dramatically improved in recent years [1]–[3]. This progress has been made possible with the rapid improvements in material quality and epitaxial layer growth techniques such as the molecular beam epitaxy (MBE) and the metallic organic chemical vapor deposition (MOCVD) [4]. However, these devices still have power limitation which are mainly attributed to the self-heating effects [5], [6] and to collector junction breakdown [7]. In general, thermal effects are significant in high power HBT's for which the dc-IV curves show strong negative slopes when biased with a high base current. It was recently reported [8] that the performance of HBT's is also affected by the environment temperature. In general, these effects are seen in a decrease of the maximum collector current as the surrounding temperature is increased.

To efficiently use HBT devices in the CAD of microwave and millimeter-wave active circuits, a compact nonlinear model, including the above effects and having a reasonable number of parameters, is needed. It is also desirable to have the same model be valid in dc, small-signal, and large-signal operating regimes. Presently, most of the models used for the analysis of the characteristics of such devices are modified versions of the Gummel–Poon (GP), model [8]–[10] which was traditionally used for silicon homojunction bipolar transistors (Si-BJTs). These GP-based circuit models do not account for the self-heating effects present in HBT's nor do they account for external temperature variation. Although remedies to this have been suggested, [11], [12] for self-heating by adding thermal circuits and [8], [11] for external temperature variation by writing explicit temperature dependence formulas for the parameters, the suggested solutions come at considerable costs in the model's complexity

and number of parameters, which in turn lead to difficulties in parameter extraction. Even with the mentioned modifications, the applicability of these models to high power devices is still questionable. Furthermore, these models often require two separate equivalent circuits [13], [14]: one for dc and large signal analyses, and a second, a linear circuit with a transconductance (g_m) and an input conductance (g_{be}), for small signal analysis at specific bias points.

In the present work, a new single nonlinear HBT model is introduced. A systematic and consistent approach for the analysis of HBT behavior under dc, small-signal, and large-signal operations is then developed using this model. The proposed model accounts for both self-heating effects and temperature dependence using a compact and explicit nonlinear equation which relates the collector current to the base current and to the collector-emitter voltage, which are the actual biasing quantities. The modeling procedure starts with the dc-IV characteristics from which the parameters of the nonlinear model are extracted. The S-parameter measurements serve then to extract the remaining extrinsic and bias dependent parameters. Once these two steps are completed, any type of analysis can be performed without the need for any additional optimizations.

The proposed model was implemented in nonlinear simulators such as SPICE [15] and HP-MDS [16]. Using the measured data for two HBT devices, the model was validated and good agreement was found in all investigated regimes of operation. In particular, harmonic-balance simulations were performed to calculate the power, gain, and power-added efficiency characteristics as well as the intermodulation distortion of the larger-size device.

II. The HBT Equivalent Circuit Model

The purpose of this work is to develop a single equivalent circuit model for HBT's that would be valid in all operating regimes. The proposed nonlinear circuit model for low power and high power HBT devices is shown in Fig. 1. The intrinsic device elements are shown within the dashed outline of Fig. 1. In the forward mode of operation, which is the mode of interest for HBT's in microwave applications, the two main nonlinearities of the device are the base-emitter diode, I_{be}, and the collector current source, I_c. The first is modeled by a physics-based diode equation of the form

$$I_{be} = I_s(e^{\alpha V_{be}} - 1) \tag{1}$$

where V_{be} is the applied base-emitter voltage (the remaining parameters are defined in the nomenclature section). The second nonlinearity, I_c, is modeled by a new empirical equation different from existing models. Since these existing models are modified forms of the Gummel–Poon model [8]–[12], they represent the collector current as a function of the base-emitter voltage, V_{be}, and the base-collector voltage, V_{bc}, (i.e., $I_c = f(V_{be}, V_{bc})$), which are not the direct biasing variables used in the device's experimental characterization. It is therefore more appropriate to derive a collector current model as a function of the biasing base current, I_b, and the biasing collector-emitter

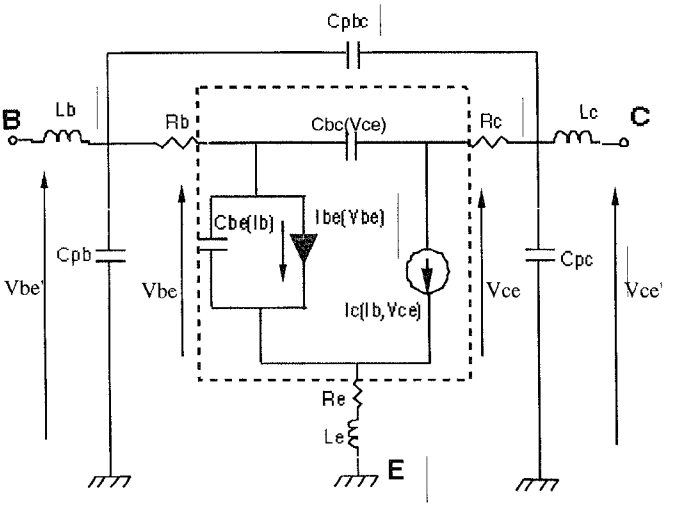

Fig. 1. The HBT nonlinear equivalent circuit.

voltage, V_{ce}, (i.e., $I_c = f(I_b, V_{ce})$). The describing function of such model is given by the empirical equation

$$I_c(I_b, V_{ce}) = X_1 \frac{\mathrm{Sinh}(X_6 + X_o V_{ce})}{(X_9 + X_o V_{ce})} \cdot \left\{ \mathrm{Sinh}\left(\frac{X_2}{I_{bn}^{X_3}} + X_4 \,\mathrm{Tanh}(X_5 I_{bn}^2) V_{ce} \right) \right\}^{\left[X_{10}\left(\frac{T-T_0}{T_0}\right)-1\right]} \tag{2}$$

where

$$X_o = X_2 + \frac{X_7}{I_{bn} V_{ce}} + \frac{X_8}{\sqrt{I_{bn}}}$$

and I_{bn} is the normalized base current

$$I_{bn} = \frac{I_b}{I_{bo}}.$$

I_{bo}	The reference base current, the lowest base current in the DC characteristics where the self-heating effects are negligible.
I_b	The base current (independent biasing variable).
V_{ce}	The collector-emitter voltage (independent biasing variable).
$X_1, \ldots, X_{10}$	The model's parameter to be extracted.
T_0	The reference temperature in Kelvin (at which $X_1, \ldots, X_9$ are extracted).
T	The analysis temperature in Kelvin.

The details of the derivation of the model (without temperature dependence) are reported in [17] and [18]. The

parameter extraction procedure is based on the optimization of the 10-parameter model of (2) against the measured dc-IV characteristics of the device at different ambient temperature settings. Equation (2) is numerically stable in dc and small-signal simulations. However, under large-signal excitations, i.e., in harmonic balance simulations, a more appropriate form that insures numerical stability is the following

$$I_c(I_b, V_{ce}) = X_1\left\{\frac{\mathrm{Sinh}(X_6)+\mathrm{Cosh}(X_6)\mathrm{Tanh}(X_oV_{ce})}{\mathrm{Cosh}(X_9)+\mathrm{Sinh}(X_9)\mathrm{Tanh}(X_oV_{ce})}\right\} \cdot\left\{\mathrm{Sinh}\left(\frac{X_2}{I_{bn}^{X_3}}+X_4\,\mathrm{Tanh}(X_5I_{bn}^2)V_{ce}\right)\right\}^{\left[X_{10}\left(\frac{T-T_0}{T_0}\right)-1\right]} \tag{3}$$

This compact model accurately accounts for both self-heating and ambient temperature effects. The self-heating effects are implicitly accounted for in the model (in the second factor of the right hand term of (2) or (3)) while the temperature dependence is explicitly represented by the power term $\left[X_{10}\left(\frac{T-T_0}{T_0}\right)-1\right]$.

The remaining intrinsic elements are the input base-emitter capacitance, C_{be}, and the feedback base-collector capacitance, C_{bc}. Both of these elements are bias dependent [19]. Their analytical expressions, as functions of I_b and V_{ce}, respectively, are described in Section IV.

The extrinsic device elements are shown outside the dashed box of Fig. 1. These elements are bias independent and represent the contact (R_b, R_c, and R_e) and the electrodes leading-pads parasitic (L_b, L_c, L_e, C_{pb}, C_{pc}, and C_{pbc}). The parameter extraction procedure for all of the presented equivalent circuit elements is outlined below.

The above-derived model is suitable for implementation in nonlinear simulators. It was successfully implemented in SPICE [17], HP-MDS and in an in-house computer program with comparable results.

III. DC Characteristics and Analysis

Two different-size GaAs HBT devices were characterized to assess the accuracy of the proposed nonlinear model. The small-size HBT is a single 15 μm^2 emitter-finger device (HBT-1), while the larger one is a 750 μm^2 emitter device (HBT-2). For dc modeling, the collector-emitter and the base-emitter I-V characteristics of the devices were measured. Table I gives some electrical properties of both devices.

The dc measured extrinsic voltages, V'_{be} and V'_{ce} shown in Fig. 1, are related to the intrinsic voltages, V_{be} and V_{ce} across the base-emitter junction and collector-emitter, respectively, by means of the series resistances R_b, R_c, and R_e as follows

$$V'_{be} - [V_{be} + I_bR_b + (I_b + I_c)R_e] = 0 \tag{4}$$

$$V'_{ce} - [V_{ce} + I_cR_c + (I_b + I_c)R_e] = 0. \tag{5}$$

The dc values of the resistances R_b, R_c, and R_e are determined from a least square minimization using (4) and (5) at different bias points. Their values are found to be almost bias independent and are listed in Table II for both devices. These values are used as initial guesses in fitting the model to the measured S-parameters as described in the next section. The measured I_{be}-V_{be} characteristics are used to extract the base-emitter diode parameters, I_s and α, while the parameters of the nonlinear collector-emitter current source, X_1 to X_{10}, were extracted using the I_c-V_{ce} characteristics. Since the collector current model (2) is temperature dependent, its parameters were extracted in two steps: first, $X_1, \cdots, X_9$ are obtained from a reference temperature measurements (in this case, $T_o = 27$°C), second X_{10} is extracted using a nonreference temperature measurements (in this case, 10°C) with $X_1, \cdots, X_9$ fixed. This parameter extraction was easily performed by fitting (1) and (2) to the measured I_{be}-V_{be} characteristics, respectively. The resulting parameters for the two devices are listed in Table II. Figs. 2 and 3 compare the room temperature measured and simulated dc-IV characteristics of the small device (HBT-1) and the large

TABLE I
SOME ELECTRICAL CHARACTERISTICS OF THE INVESTIGATED HBT DEVICES; HBT-1: EMITTER AREA: 15 μm^2; HBT-2: EMITTER AREA: 750 μm^2

CHARACTERISTICS	HBT-1	HBT-2
Total emitter area: A_E	15 μm^2	750 μm^2
Current density: J	3.5x10^4 A/cm^2	4x10^4 A/cm^2
DC current gain: b	38-41	50-55
Cut-off frequency: f_T	28.5 GHz	8 GHz
Oscill. frequency: f_{max}	45 GHz	12 GHz

TABLE II
MODEL'S PARAMETERS OF THE NONLINEAR COLLECTOR CURRENT AND BASED-EMITTER DIODE OF THE DEVICES HBT-1 AND HBT-2

Parameters	HBT-1	HBT-2
R_b	44.3 Ω	4.95 Ω
R_c	8.25 Ω	0.97 Ω
R_e	5.5 Ω	0.91 Ω
X_1	0.000146	0.00106
X_2	0.926	1.3254
X_3	1.05	1.2073
X_4	-0.0028	0.008055
X_5	792.2	0.4424
X_6	-0.748	0.5332
X_7	-3.54	-2.1493
X_8	10.3	10.0516
X_9	-2.37	-2.0165
X_{10}	0.434	0.614
α	10.34	6.51
I_s	4.26x10^{-12}	7.82x10^{-8}

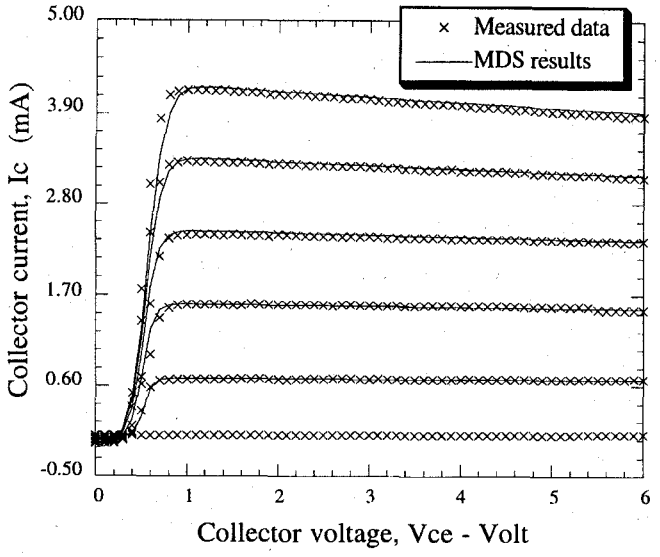

Fig. 2. Simulated and measured dc-IV characteristics of the HBT-1 device.

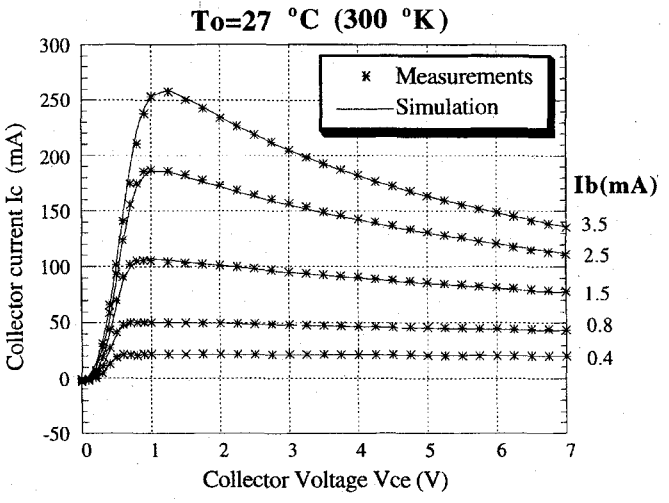

Fig. 3. Simulated and measured dc-IV characteristics of the HBT-2 device.

device (HBT-2), respectively. One can see that the model's results are in good agreement with the measured data in all operating regions of the devices, and the strong negative slopes in the curves of HBT-2 are accurately represented by the model.

To study the validity of the model at different ambient temperatures, the measured dc characteristics of HBT-2 at different temperatures were compared to the simulated results using the parameters of Table II. The results are shown in Fig. 4 for a temperature of 50°C and show good accuracy. Similar results were obtained at other temperatures.

IV. Small-Signal Modeling and Analysis

The S-parameters of both devices (HBT-1 and HBT-2) were measured at various bias points concentrated mainly in the forward active region (base-emitter junction is forward biased, and base-collector junction reverse biased), which is of primary importance for microwave active circuits and is

TABLE III
Extrinsic and Intrinsic Parameters of the Model for HBT-1 and HBT-2.

Parameters	HBT-1	HBT-2
L_b	0.043 nH	0.691 nH
L_c	0.061 nH	0.091 nH
L_e	0.034 nH	0.038 nH
R_b	47.2 Ω	5.198
R_c	1.8 Ω	10.2
R_e	6.7 Ω	1.5
C_{pbc}	0.021 pF	0.71 pF
C_{pb}	0.038 pF	-
C_{pc}	0.023 pF	-
a_1	0.12	0.06
a_2	9.25	0.255
b_1	0.1	0.01
b_2	52.3	4.9
C_{bo}	-	0.102 pF
C_{co}	-	0.216 pF
L_{bo}	-	0.01 nH
L_{co}	-	0.298 nH

associated with maximum efficiency of operation. For small-signal modeling, the same HBT equivalent circuit of Fig. 1 is used. One aspect of the consistency of the proposed model resides in the fact that the parameters of the collector current (2) and those of the diode (1) obtained from dc measurements are fixed. The remaining extrinsic elements are then determined by fitting the calculated to the measured S-parameters at different bias points using a gradient optimization procedure. As expected, the extrinsic parasitic elements were found to exhibit little bias dependence. The results of this optimization are summarized in Table III for both devices. In addition, from multibias S-parameter fittings, the bias-dependence of the intrinsic capacitances, C_{be} and C_{bc}, which is of the form

$$C_{be} = a_1 + a_2 I_b \, pF \tag{6}$$

and

$$C_{bc} = \frac{1}{(b_1 + b_2 V_{ce})} \, pF \tag{7}$$

is obtained, where the base current I_b, is in mA and the collector-emitter voltage, V_{ce}, is in Volts. The parameters, a_1, a_2, b_1, and b_2, for these capacitances, obtained after curve fitting, are listed in Table III. Based on these results, C_{be} is found to be strongly dependent on the base current, I_b, while C_{bc} has a hyperbolic dependence on V_{ce} which is consistent with the explanations of [15] stating that C_{bc} increases at

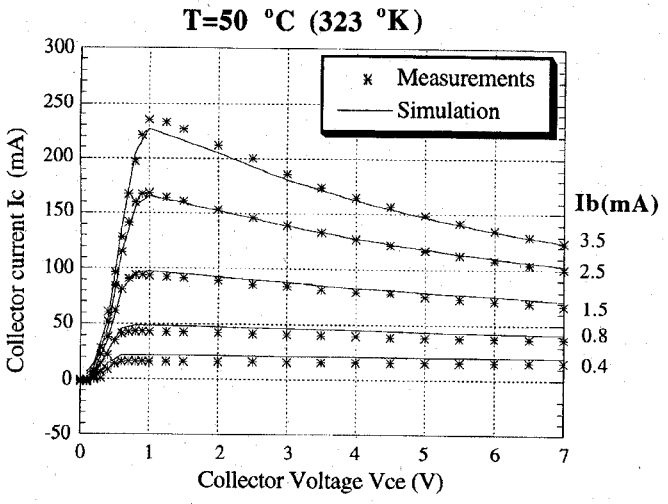

Fig. 4. Predicted and measured dc-IV characteristics of HBT-2 at $T = 50°C$ (323° K).

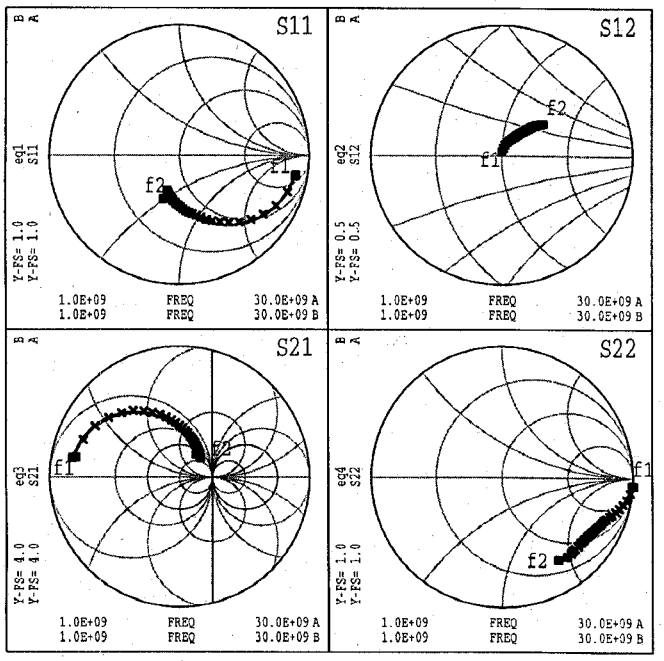

Fig. 5. Simulated and measured S parameters of HBT-1; bias: $I_b = 120$ μA, $V_{ce} = 4.5$ V.

low collector-emitter voltages due to the base-charge increase caused by the HBT beginning to enter the saturation region.

Using the model parameters derived from the dc and small-signal measurements as described above, the S-parameters of HBT-1 and HBT-2 were obtained by simulation at different bias points over the frequency ranges of 1 to 30 GHz and 1 to 8 GHz, respectively. The HBT-2 packaged device were measured up to 8 Ghz due to the limited operational frequency range of the in house made fixture. The results are presented in Figs. 5 and 6 and show excellent agreement between measurement and simulation at the bias point chosen with similar agreement at other biasing conditions. It should be noted that since HBT-2 is a packaged device, parasitic elements were

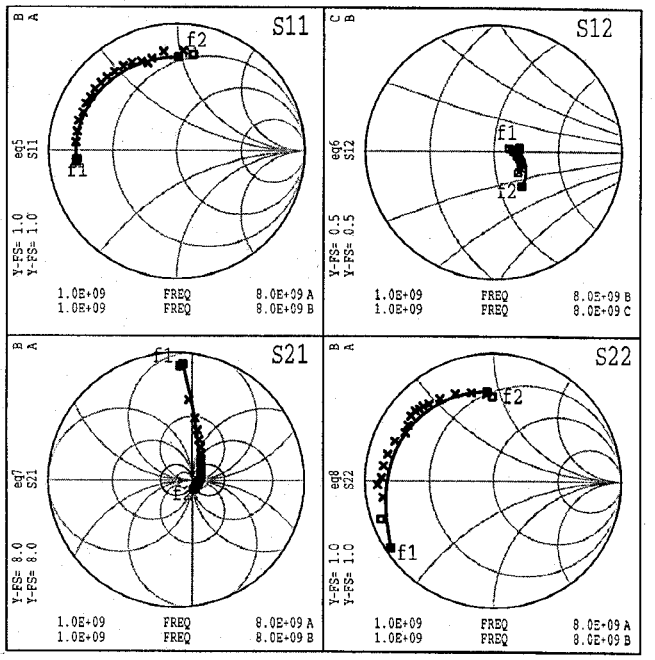

Fig. 6. Simulated and measured S parameters of HBT-2; bias: $I_b = 4.5$ mA, $V_{ce} = 5.0$ V.

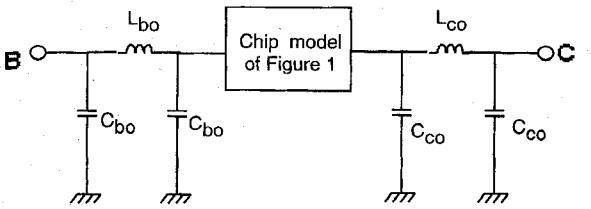

Fig. 7. Equivalent model of the packaged device HBT-2.

added to the model of Fig. 1 as shown in Fig. 7. The extracted values of these parasitics are listed in Table III.

V. Power Characteristics and Harmonic Balance Analysis

The output powers at the fundamental frequency and its higher order harmonics versus input power characteristics were measured using the HP microwave transition analyzer (HP70004A MTA). The measurements were performed on the packaged large-size device, HBT-2, at the fundamental frequency of 2 GHz. The output versus input power characteristics, for 50 Ω source and 50 Ω load, were measured at various dc bias points. The large-signal characteristics of the device were simulated using the nonlinear equivalent circuit of Fig. 7, with (3), implemented in HP-MDS without any additional modifications or optimizations, which is another aspect of the consistency of the proposed model. The harmonic balance simulation technique [20], [21] was used to calculate the device's output power and gain characteristics as functions of the input power at the corresponding bias points. Three harmonics were considered and were found to be sufficient for accurate calculations.

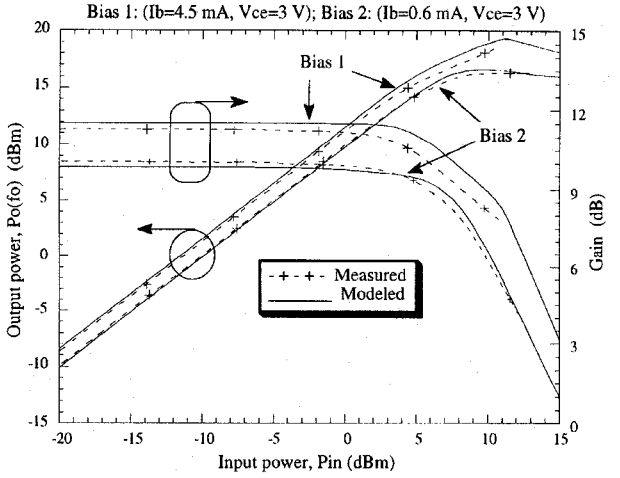

Fig. 8. Measured and simulated output power and gain vs input power for HBT-2 at two bias cases and with 50 Ω terminations; bias 1: $I_b = 4.5$ mA, $V_{ce} = 3.0$ V, bias 2: $I_b = 0.6$ mA, $V_{ce} = 3.0$ V.

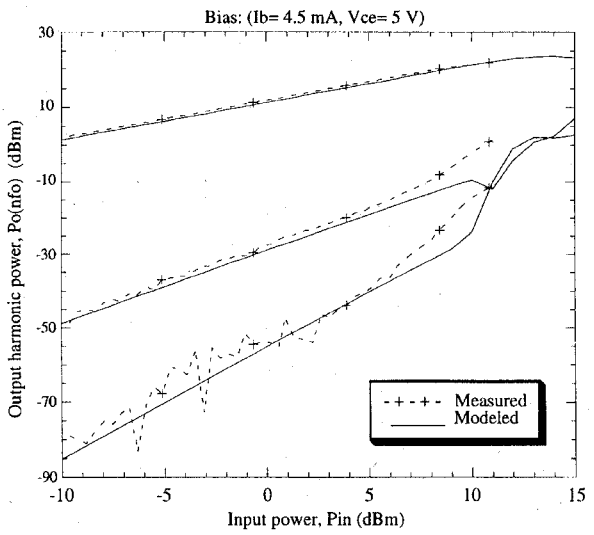

Fig. 9. Measured and simulated output power harmonics; $I_b = 4.5$ mA, $V_{ce} = 5.0$ V.

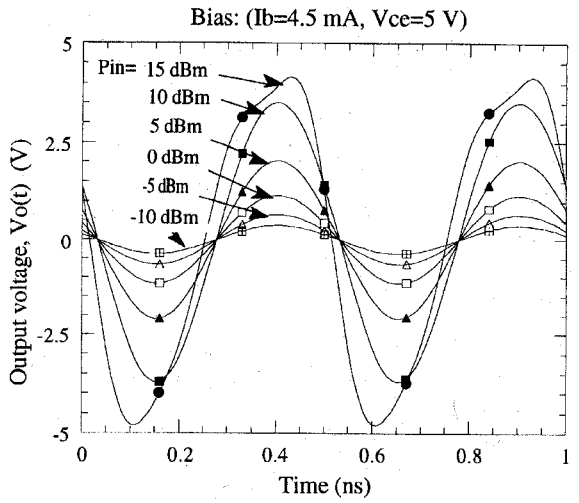

Fig. 10. Output waveforms in 50 Ω load for different input excitations; bias: $I_b = 4.5$ mA, $V_{ce} = 5.0$ V.

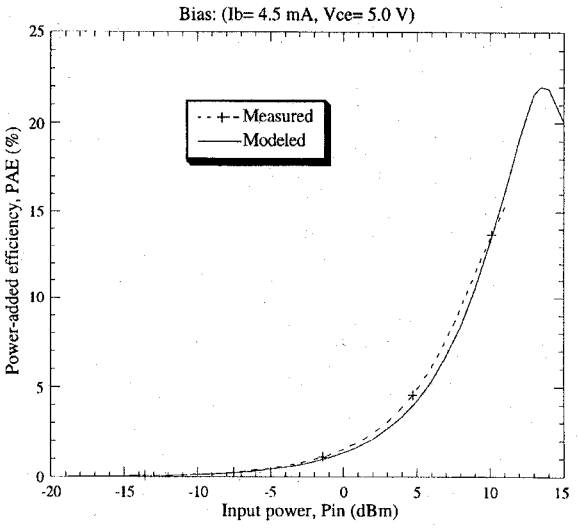

Fig. 11. Measured and simulated power-added efficiency versus input power; bias: $I_b = 4.5$ mA, $V_{ce} = 5.0$ V.

Fig. 8 shows the measured and calculated power and gain characteristics at two bias points for HBT-2. The first bias point ($I_b = 4.5$ mA, $V_{ce} = 3$ V) corresponds to class A operation while the second point ($I_b = 0.6$ mA, $V_{ce} = 3$ V) corresponds to class AB operation. As expected, the compression point of the device, operating in class AB, occurs at an input power level lower than in class A operation. A comparison between the simulated and the measured output power of the harmonics when the device is biased in class A operation is shown in Fig. 9. It is clear that the model accurately predicts the three output harmonic power levels over 20 dB dynamic range. The noise in the measured $P_o(3f_o)$ at low input power levels may be due to the limited detection sensitivity of the MTA at low power levels. With 50 Ω terminations, the effects of the device's nonlinearities are minimal. This can be seen in Fig. 9 where the second and third harmonic levels are at least 15 dB below the fundamental level. This can also be seen in output voltage waveforms of Fig. 10, where the saturation starts to take place at $P_{\text{in}} = 10$ dBm.

To further assess the accuracy of the model, the power-added efficiency (PAE) is computed. The PAE of the device is defined as the ratio of the additional power provided by the device to the dissipated dc power, P_{dc}, [13]

$$\text{PAE} = \frac{P_L - P_{\text{in}}}{P_{dc}} \tag{8}$$

where P_L is the power absorbed by the load and P_{in} is the RF input power. This characteristic was calculated using the harmonic balance simulation results. In particular, the dc power is calculated using the dc components of the collector current and the collector-emitter voltage spectra ($P_{dc} = V_{ce}I_c$). Fig. 11 shows the measured and calculated PAE of the device versus the input power under 50 Ω terminations. Good agreement between measurement and simulation is once again obtained confirming the validity and the robustness of the proposed

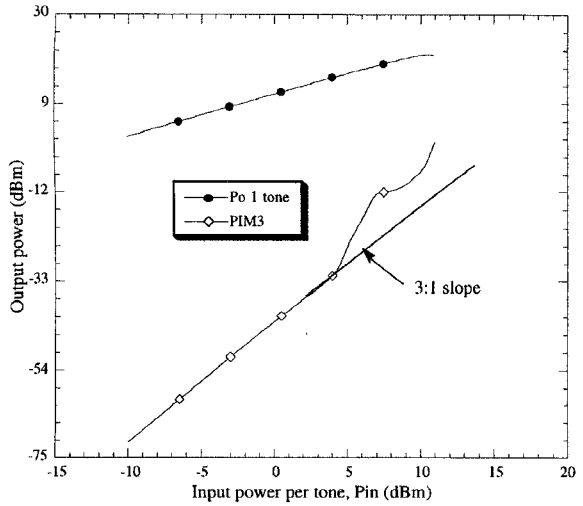

Fig. 12. Intermodulation distortion simulation results: Output power per tone and third-order intermodulation distortion versus input power per tone.

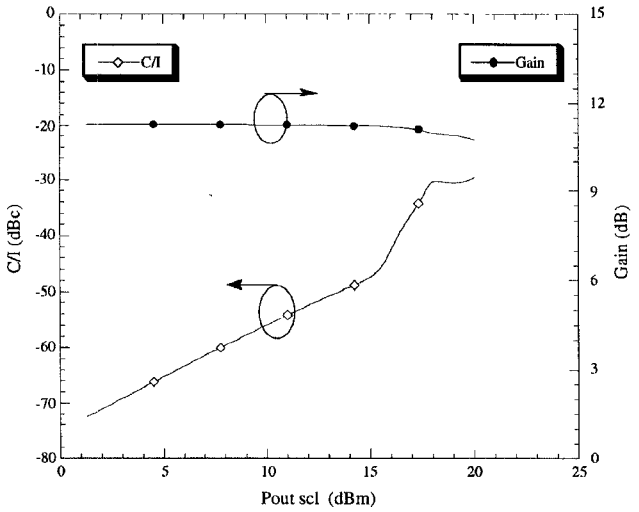

Fig. 13. Intermodulation distortion simulation results: C/I (IM_3) and gain versus single carrier output power.

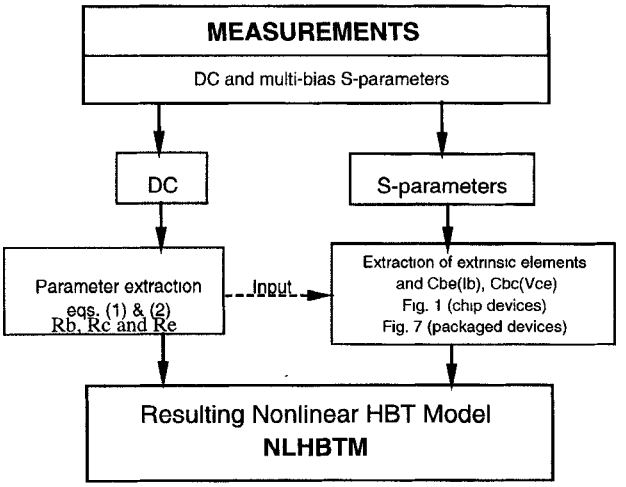

(a)

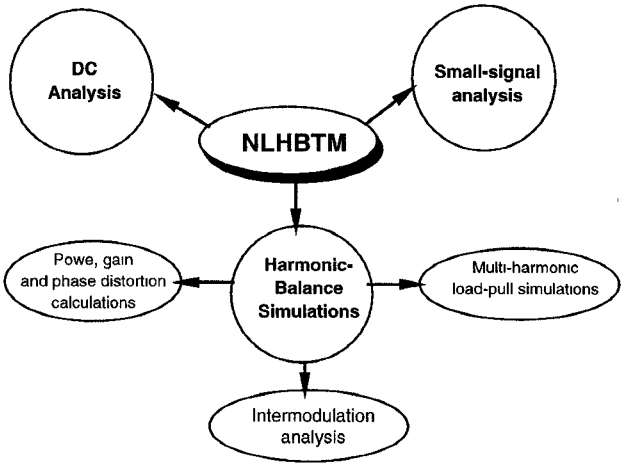

(b)

Fig. 14. Phases of the modeling, parameter extraction and analysis for the new model. (a) Phase I: Modeling and parameter extraction. (b) Phase II: Possible analysis options.

model which accurately predicts the dc behavior even if a large-signal RF drive is present at the input of the device.

The consistency of the model is further tested via intermodulation distortion analysis which is a good test for device's linearity, an important requirement for multicarrier or time varying signal applications. This was accomplished by examining the ratio of the carrier level to the third-order product level (C/I_3) under two-tone excitation. This test was carried out at carrier frequencies of 2.0 and 2.005 GHz with equal amplitudes. The two-tone simulation results, in class A operation and with 50 Ω terminations are illustrated in Figs. 12 and 13. Fig. 12 shows the single carrier output power and the third-order intermodulation distortion ($P_{IM3} = P_o(2f_1 + f_2)$) as functions of the input power per tone. As observed in [22], the third-order intermodulation distortion increases faster than a 3:1 slope at higher power levels. This is due to the fact that the transistor is approaching the 1-dB compression point where the device's large-signal nonlinearities start to take effect. Fig. 13 shows the C/I_3 level and the gain as functions of the single carrier output power. One can see that a good C/I_3 of -25 dBc is obtained at the device's 1 dB compression point while a C/I_3 better than -35 dBc is attainable at 2 dB backoff from the P_{1dB} compression point. This confirms the higher linearity achievable with HBT's compared to MESFET's [22].

VI. Summary

The proposed model and the systematic approach for its parameter extraction and its application to dc, small-signal, and large-signal single and multitone analysis can be summarized in the flow-chart format of Fig. 14. Starting with the measured dc-IV curves, the parameters of the nonlinear elements of (1) and (2) are extracted. The results of this first step are combined, unmodified, with the multibias S-parameter measurements for the extraction of the remaining equivalent circuit elements. At the end of this step, i.e., end of phase I of Fig. 14(a), the HBT model is complete. The model can then

be used for simulation under any operating mode as shown in Fig. 14(b) without any modifications.

VII. Conclusion

The dc, small-signal, and large-signal characteristics of HBT's were investigated using a new consistent nonlinear model. The model accounts for the self-heating effects as well as the environmental temperature dependence. In addition to accuracy, the model offers the advantage that it is a function of the independent biasing variables (I_b and V_{ce}), making it appropriate for direct comparison with measured data. The parameters of the equivalent circuit of the model were extracted from measured dc and S-parameters. The proposed model was easily implemented in HP-MDS as well as a personal computer code. The simulations performed using the nonlinear model have provided computed dc, small-signal, and large-signal characteristics which are in good agreement with the measured results for the different size HBT's investigated. The power-saturation mechanisms have been shown to be dependent on the class of operation and the termination conditions. Good HBT linearity, compared to MESFET's, has been observed via intermodulation distortion analysis showing low third-order intermodulation distortion power levels and, consequently, very low C/I_3 levels.

Acknowledgment

The authors wish to thank F. Beauregard for his helpful discussions and assistance during the characterization and the mounting of the device.

References

[1] K. Fricke *et al.*, "Performance capabilities of HBT devices and circuits for satellite communication," *IEEE Trans. Microwave Theory Tech.*, vol. 40, no. 6, pp. 1205–1214, June 1992.

[2] M. E. Kim *et al.*, "GaAs heterojunction bipolar transistor device and IC technology for high-performance analog and microwave applications," *IEEE Trans. Microwave Theory Tech.*, vol. 37, no. 9, pp. 1286–1302, Sept. 1989.

[3] P. M. Asbeck *et al.*, "Heterojunction bipolar transistors for microwave and millimeter-wave integrated circuits," *IEEE Trans. Microwave Theory Tech.*, vol. 35, no. 12, pp. 1462–1470, Dec. 1987.

[4] F. Ali and A. Gupta, *HEMTs & HBTs: Devices, Fabrication and Circuits.* Norwood, MA: Artech House, 1991.

[5] R. C. Joy and E. S. Schlig, "Thermal properties of very fast transistors," *IEEE Trans. Electron Devices*, vol. 17, pp. 586–594, Aug. 1970.

[6] S. P. Gaur, D. H. Navon, and R. W. Teerlinck, "Transistor design and thermal stability," *IEEE Trans. Electron Devices*, vol. ED-20, pp. 527–534, June 1973.

[7] P. L. Hower and V. G. K. Reddi, "Avalanche injection and second breakdown in transistors," *IEEE Trans. Electron Devices*, vol. ED-17, pp. 320–335, Apr. 1970.

[8] C. T. Dikmen, N. S. Dogan, and M. A. Osman, "DC Modeling and characterization of AlGaAs/GaAs heterojunction bipolar transistors for high-temperature applications," *IEEE J. Solid State Circuits*, vol. 29, no. 2, pp. 108–116, Feb. 1994.

[9] M. E. Hafizi, C. R. Crowell, and M. E. Grupen, "The dc characteristics of GaAs/AlGaAs heterojunction bipolar transistors with application to device modeling," *IEEE Trans. Electron Devices*, vol. 37, no. 10, pp. 2121–2129, Oct. 1990.

[10] J. Rodriguez-Tellez, "New nonlinear large-signal dc bipolar junction transistor model," *IEE Proc.-G*, vol. 138, no. 2, pp. 145–150, Apr. 1991.

[11] P. C. Grossman and A. Oki, "A large-signal dc model for GaAs/$Ga_{1-x}Al_xAs$ heterojunction bipolar transistors," in *IEEE Bipolar Circuits and Technol. Meet. Dig.*, Sept. 18–19, 1989, pp. 258–261.

[12] P. C. Grossman and J. Choma, "Large signal modeling of HBT's Including self-heating and transit time effects," *IEEE Trans. Microwave Theory Tech.*, vol. 40, no. 3, pp. 449–464, Mar. 1992.

[13] M. Y. Frankel and D. Pavlidis, "An analysis of the large-signal characteristics of AlGaAs/GaAs heterojunction bipolar transistors," *IEEE Trans. Microwave Theory Tech.*, vol. 40, no. 3, pp. 465–474, Mar. 1992.

[14] D. A. Teeter, J. R. East, and G. I. Haddad, "Large-signal HBT characterization and modeling at millimeter wave frequencies," *IEEE Trans. Microwave Theory Tech.*, vol. 41, no. 6/7, pp. 1087–1093, June/July 1993.

[15] HSPICE Users' Manual, Meta-Software, Inc. June 1987.

[16] HP85150 Microwave Design System (MDS), *Building and Analyzing Circuits*, Hewlett Packard, USA May 1990.

[17] J. Dupuis *et al.*, "A new dc model of HBT's including self-heating effect suitable for circuit simulators," *IEEE Trans. Electron Devices*, vol. 42, no. 12, pp. 2036–2042, Dec, 1995.

[18] J. Dupuis and F. M. Ghannouchi, "Modélisation dc des transistors bipolaires à hétérojonction," 8ème J. Nationales Microondes, Brest 12–14 May 1993, France, pp. 6A/2-6A/3.

[19] R. Hajji and F. M. Ghannouchi, "On the use of S-parameter measurements to model HBT intrinsic elements for large-signal analysis purposes," *Microwave and Opt. Technol. Lett.*, vol. 6, no. 10, pp. 605–607, Aug. 1993.

[20] S. A. Maas, *Nonlinear Microwave Circuits.* Norwood, MA: Artech House, 1988.

[21] V. Rizzoli and A. Neri, "State of the art and present trends in nonlinear microwave CAD techniques, *IEEE Trans. Microwave Theory Tech.*, vol. 36, pp. 343–365, Feb. 1988.

[22] N. L. Wang, W. J. Ho, and J. A. Higgings, "AlGaAs/GaAs HBT linearity characteristics," *IEEE Trans. Microwave Theory Tech.*, vol. 42, no. 10, pp. 1845–1850, Oct. 1994.

Rached Hajji (S'94–M'95) was born in 1964, in Nefta, Tunisia. He received the B. Ing., M.Sc.A., and Ph.D. degrees in electrical engineering from École Polytechnique de Montréal, Canada in 1988, 1990, and 1995, respectively.

From 1990 to 1991, he was a Research Assistant at the Microwave Research Laboratory of École Polytechnique de Montréal working on the characterization and modeling of GaAs MESFET's. His research interests include the characterization and modeling of microwave and millimeter-wave low-power and high-power semiconductor active devices including GaAs MESFET's and heterojunction bipolar transistors. He is currently working in APMLI project in the École Polytechnique of Montreal as post-doctoral fellow.

Dr. Hajji was the recipient of the National Scholarship from the Tunisian government from 1984 to 1990.

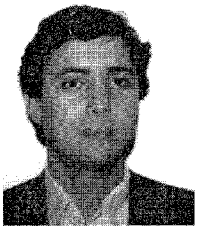

Ammar B. Kouki (S'88–M'92) was born in Téboursouk, Tunisia. He received the B.S. and M.S. degrees in engineering science from the Pennsylvania State University, University Park, PA, in 1985 and 1987, respectively. He received the Ph.D. degree in electrical engineering from the University of Illinois at Urbana-Champaign in 1991.

From 1985 to 1987 he was a Research Assistant with the Research Center for the Engineering of Electronic and Acoustic Materials at the Pennsylvania State University. From 1987 to 1991 he was a Research Associate with the Electromagnetic Communications Laboratory at the University of Illinois. Since 1991, he has been with the Microwave Research Laboratory at L'École Polytechnique de Montréal. His research interests include the application of integral equation and finite element techniques to the analysis of passive microwave circuits, finite element and finite difference modeling of nonlinear devices, experimental and numerical characterization of the EMC and EMI properties of printed circuits, scattering from rough surfaces, RCS calculation and the development of Graphical User Interfaces for electromagnetic analysis programs using X-Windows and Motif.

Dr. Kouki was the recipient of the National Scholarship from the Tunisian government from 1981 to 1991 and is a member of Tau Beta Pi.

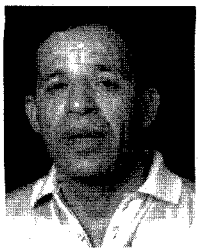

Sayed El-Rabaie (M'88) received the degree in electrical engineering in 1976 from Tanta University, Egypt. In 1981, he received the M.Sc. degree in communication systems in Menoufia University, Egypt. He then received the Ph.D. degree in microwave device engineering from the Queen's University of Belfast, U.K., in 1986. From 1986 to 1988, he was a post-doctoral fellow with the Device Simulation Group of the electrical and electronic engineering department of Belfast University, U.K.

Since 1989 he has been a Professor in the Department of Communications Engineering, Faculty of Electronic Engineering, Menouf, Egypt. His main research interests are in microwave nonlinear device modeling, simulation and design. During the summer of 1994, he was in the microwave research laboratory of Ecole Polytechnique of Montreal, Canada as an invited professor, where he worked on the modeling and simulation of GaAs-MESFET's and GaAs-HBT's.

Fadhel M. Ghannouchi (S'84–M'88–SM'93) received the degree in physics/chemistry in 1980 from the University of Tunis. He then received the B.Eng. degree in engineering physics in 1983 and the M.Eng. and Ph.D. degrees in electrical engineering in 1984 and 1987, respectively, from Ecole Polytechnique de Montreal, Montreal, Canada.

He is currently an Associate Professor with the Electrical Engineering Department at Ecole Polytechnique de Montreal where he has been teaching electromagnetics and microwave theory and techniques since 1984. His research interests are microwave/millimeter-wave instrumentation and measurements. He conducted several research projects that led to the design and construction of several six-port network analyzers over the 0.5–40 GHz range. He extended the six-port techniques from standard S-parameter measurements to large-signal (multi-harmonic load-pull) and pulse characterization of microwave active devices. His other research interests are in the area of nonlinear modeling of microwave and millimeter-wave devices and to the control and calibration of phased array antennas.

Dr. Ghannouchi is a registered Professional Engineer in the province of Quebec, Canada. He is on the editorial board of IEEE TRANSACTIONS ON MICROWAVE THEORY AND TECHNIQUES and he served on the technical committees of several international conferences and symposiums and provide consulting services to a number of microwave companies.